ChemComm

COMMUNICATION

View Article Online
View Journal | View Issue

Cite this: *Chem. Commun.*, 2020, **56**, 1541

Received 2nd October 2019,
Accepted 23rd December 2019

DOI: 10.1039/c9cc07748k

rsc.li/chemcomm

A nickel coordination polymer derived from 1,2,4,5-tetraaminobenzene for fast and stable potassium battery anodes†

Roman R. Kapaev, *[abc] Ivan S. Zhidkov,[d] Ernst Z. Kurmaev,[de] Keith J. Stevenson[a] and Pavel A. Troshin[ab]

We report the application of a Ni-based coordination polymer derived from 1,2,4,5-tetraaminobenzene (P1) as a fast and stable potassium battery anode. In a voltage range of 0.5–2.0 V *vs.* K^+/K, a reversible capacity of 220 mA h g^{-1} was obtained at 0.1 A g^{-1}. Even with a relatively high electrode loading of 5.0 mg cm^{-2} and only 10 wt% carbon additive, 118 mA h g^{-1} was still retained at 1 A g^{-1}. For thinner electrodes with 30 wt% carbon, a capacity of up to 104 mA h g^{-1} was observed at 10 A g^{-1} (charging in ~40 seconds). An areal capacity of up to 2.73 mA h cm^{-2} was demonstrated. The capacity fade at 1 A g^{-1} was only 4.4% after 200 cycles. Structure transformations of P1 during charge/discharge were studied using X-ray photoelectron spectroscopy and *in situ* X-ray diffraction.

K-ion batteries (KIBs) have attracted great attention as alternatives to Li-ion batteries (LIBs), which are now commercialized and widely appied.[1–4] Potassium is much more abundant than lithium, which makes KIBs potentially more sustainable compared to LIBs.[1] The diffusion coefficients for K^+ in electrolytes are typically higher than those for Li^+,[2] which might help in improving the rate capabilities of the batteries, provided that the active materials themselves have fast charge–discharge kinetics.

Various materials have been proposed to make anodes of KIBs – carbons,[5,6] aryl carboxylates,[7,8] potassium titanates[9,10] and others.[3,11] However, anode materials that operate at high charge/discharge rates (charging in <5 min) are still underrepresented. In addition, the potentials of the anode materials in the metalated state stay at ~0 V *vs.* K^+/K in most of the reports. Operation at such low potentials might lead to safety issues due to the high chemical reactivity of the metalated anodes.[12] Moreover, there appears a risk of potassium metal deposition caused by overcharge, operation at low temperatures or high charge–discharge rates; the alkali metal tends to form dendrites, which might cause dangerous short-circuiting of the cells.[13,14] For LIBs, there is a widely studied family of lithium titanates working in safer voltage windows, *e.g.* 1.0–2.5 V[15] or 0.5–2.0 V[16] *vs.* Li^+/Li.[12] For K-ion batteries, materials with similar redox potentials along with relatively high capacity (>170 mA h g^{-1}) and excellent rate capability have been unknown.

Recently, linear Ni-based coordination polymer **P1** (Fig. 1) has been proposed as an anode material for lithium- or sodium batteries with fast (charging in <2 min) charge/discharge capabilities.[17,18] The polymer was shown to be redox-active in the voltage range between *ca.* 0.5 and 2.0 V *vs.* Li^+/Li or Na^+/Na, and demonstrated decent stability over thousands of charge–discharge cycles. Considering these results, we hypothesized that **P1** might also be used as a fast and stable anode material for potassium-ion batteries operating in a safe voltage window.

P1 was synthesized according to a previously reported procedure,[17] and no post-synthetic treatment such as ball-milling was applied. We evaluated the material in half-cells using potassium as an anode and 1.5 M solution of KPF_6 in 1,2-dimethoxyethane as electrolyte (see details in the ESI†). The voltage range was 0.5–2.0 V *vs.* K^+/K. The electrode contained **P1**, Super P and CMC at a 6 : 3 : 1 weight ratio, and the **P1** areal loading was ~1.0 mg cm^{-2}. The capacity of Super P was shown to be <50 mA h g^{-1} in the selected voltage range (Fig. S1, ESI†).

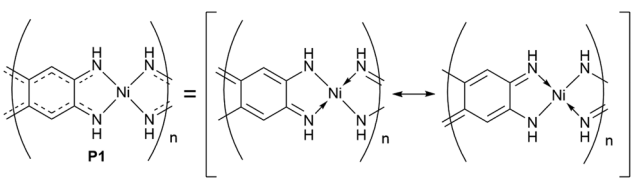

Fig. 1 Structural formula and resonance structures of **P1**.

[a] *Center for Energy Science and Technology, Skolkovo Institute of Science and Technology, Nobel str. 3, Moscow 143026, Russia. E-mail: roman.kapaev@skoltech.ru*
[b] *Institute for Problems of Chemical Physics RAS, Acad. Semenov str. 1, Chernogolovka 142432, Russia*
[c] *D.I. Mendeleev University of Chemical Technology of Russia, Miusskaya sq. 9, Moscow 125047, Russia*
[d] *Institute of Physics and Technology, Ural Federal University, Mira str. 19, Yekaterinburg 620002, Russia*
[e] *M.N. Mikheev Institute of Metal Physics of Ural Branch of Russian Academy of Sciences, S. Kovalevskoi str. 18, Yekaterinburg 620108, Russia*

† Electronic supplementary information (ESI) available. See DOI: 10.1039/c9cc07748k

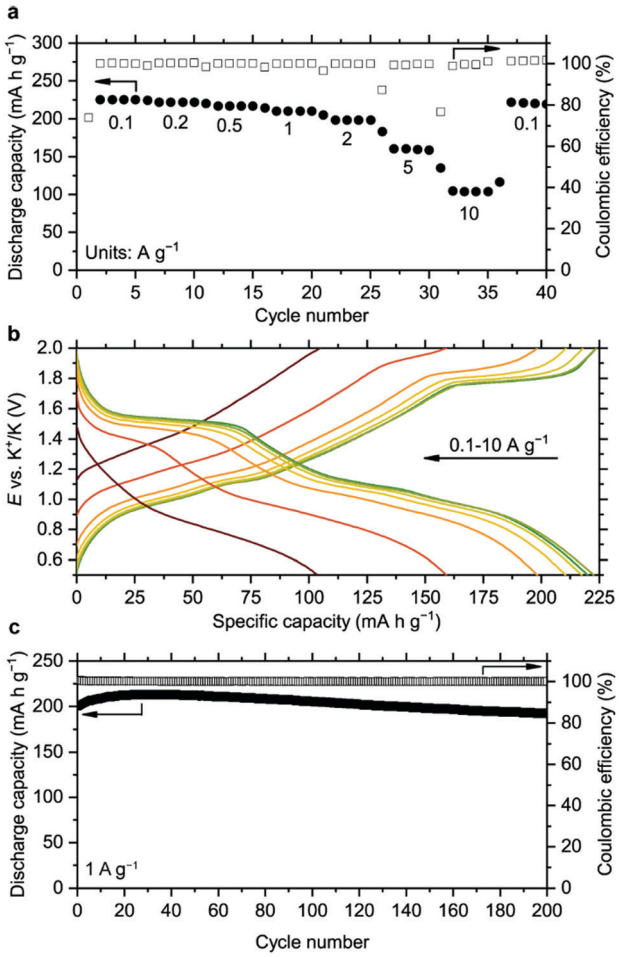

Fig. 2 Rate and cycle performance of **P1**: (a) discharge capacities and coulombic efficiencies at different current densities; (b) charge–discharge curves of **P1** for each 5th cycle shown in (a) except for cycle 5; and (c) cycling stability at 1 A g^{-1}.

The contribution to the capacity from Super P was subtracted from the charge–discharge curves of **P1** (the charge–discharge curves before and after subtraction are shown in Fig. S2, ESI†).

As depicted in Fig. 2a and b, **P1** showed a high reversible capacity of 220 mA h g^{-1} at 0.1 A g^{-1} (charging in ~2.4 h). The capacity per total electrode mass was 145 mA h g^{-1} (the current density per electrode mass was 0.06 A g^{-1}). The average depotassiation potential was 1.36 V *vs.* K$^+$/K. This makes the material suitable for anodes that might be paired with high voltage cathode materials, such as Prussian blue analogs,[19] polyanionic compounds[20] or dihydrophenazine-based polymers.[21] The polymer demonstrated excellent rate capability, with 104 mA h g^{-1} observed even at 10 A g^{-1} (65 mA h g^{-1} per total electrode mass, charge/discharge in ~40 seconds).

This is the best result in terms of specific capacity and fast charge–discharge for potassium battery anode materials, which operate above 0.5 V *vs.* K$^+$/K (see the comparison with the benchmarks[22,23] in Fig. S3, ESI†). Although some materials, such as bismuth[24,25] or phosphorus,[26–28] have higher capacities and should provide higher full cell voltages, all of them have to be potassiated at low potentials (typically ~0 V *vs.* K$^+$/K), which is associated with safety concerns as discussed above.

The cycling stability was tested at 1 A g^{-1} current density (charging in ~14 min). Prior to cycling, the material was pre-conditioned by performing the first discharge–charge–discharge sequence at 0.1 A g^{-1} to eliminate capacity depression related to the low initial conductivity of **P1**.[17] The polymer showed decent cycling stability, with only 4.4% fade after 200 cycles (Fig. 2c).

To improve the overall electrode capacity, we decreased the Super P content from 30 to 10% wt. With roughly the same **P1** areal loading (1.3 mg cm^{-2}), the material still showed decent rate capabilities, with 182 mA h g^{-1} observed at 1 A g^{-1} (Fig. S3 and S4, ESI†). The charge–discharge profiles remained virtually unchanged (Fig. S5, ESI†). By increasing the electrode areal loading to 5.0 and 15.2 mg cm^{-2}, the areal capacity could reach 0.90 and 2.73 mA h cm^{-2}, respectively (Fig. S6, ESI†). Even with a high loading of 5.0 mg cm^{-2} and only 10 wt% Super P, the specific capacity approached 118 mA h g^{-1} at 1 A g^{-1} (Fig. S3, ESI†).

The cyclic voltammogram in Fig. 3 revealed four cathodic and three anodic peaks for **P1**. The fourth anodic peak was unobserved possibly due to the overlapping with the peak at ~1.14 V. The overpotential for a pair of peaks appearing at >1.4 V was several times higher than those for the other peaks. Such behavior along with characteristic plateaus observed in the charge–discharge curves (Fig. 2b) might indicate a phase transition.[29]

To support this hypothesis, we measured *in situ* X-ray diffraction (XRD) patterns of a **P1**-based electrode during discharge (see the procedure in the ESI†). In the initial state, two peaks were observed at 2θ ~21° and ~24°, which correspond to **P1**[17] (Fig. 4). At 1.4–1.0 V *vs.* K$^+$/K, these peaks disappeared without shifting, confirming a phase transition. At ~1.0 V, another peak appeared at ~25° and then gradually shifted to ~23.5° upon discharging to 0.5 V, indicating a solid-solution mechanism.[30]

To further investigate the redox processes of **P1** in potassium half-cells, we measured X-ray photoelectron spectra (XPS) of electrodes in charged and discharged states. For the C 1s spectra, contributions from the C=N and C–N of the polymer[18] can be

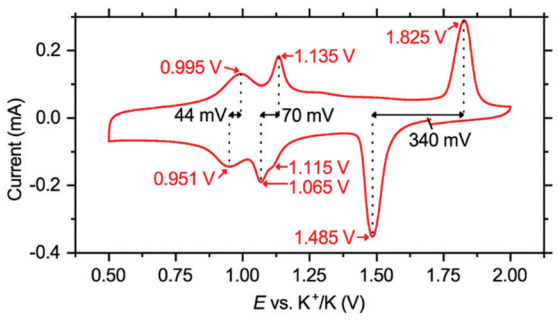

Fig. 3 Cyclic voltammogram for a **P1**//K half-cell at 0.2 mV s^{-1}. Prior to performing the scan, the cell was subjected to 20 pre-conditioning scans at 1 mV s^{-1} to eliminate all irreversible redox reactions, and left at an open-circuit voltage for 12 hours.

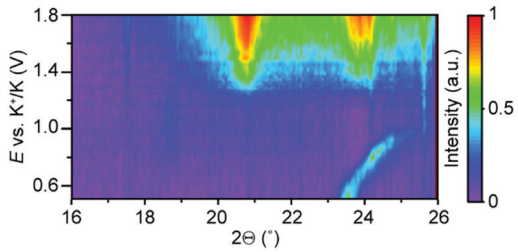

Fig. 4 *In situ* XRD patterns of a **P1**//K half-cell during the initial discharge. The background signal, which was constant upon discharge, was subtracted from the patterns.

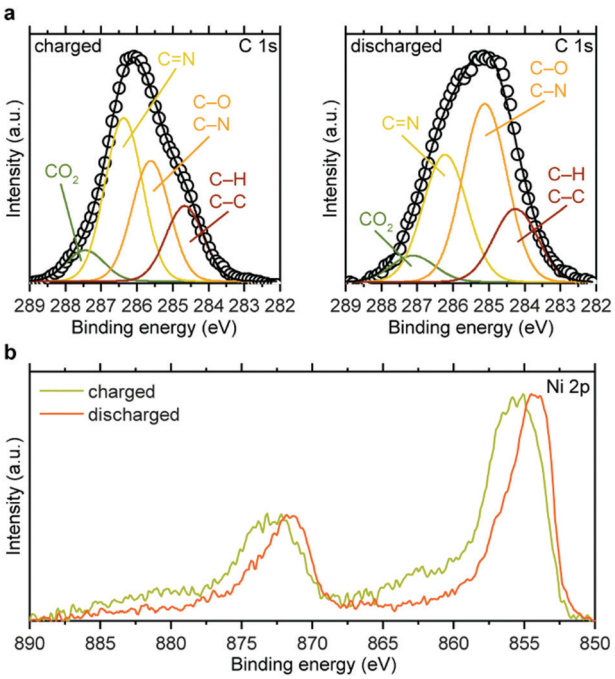

Fig. 5 XPS profiles for **P1**-based electrodes: (a) C 1s and (b) Ni 2p spectra for charged and discharged states. Experimental data points for (a) are shown in circles, and the overall fit curves are shown as black lines.

distinguished along with the C–O/CO_2 groups of the sodium carboxymethyl cellulose binder and the C–C/C–H groups of the carbon and binder additives[31–33] (Fig. 5a). In the discharged state, the contribution from the C=N groups was lower compared to the discharged state, which suggests the reduction of the ligand upon potassiation.[18]

In the Ni 2p spectra in Fig. 5b, a shift to lower binding energies was observed upon discharge, which was due to the increased negative charge on the polymer backbone. However, there was no evidence of Ni(II) transition to lower oxidation states. In the discharged state, the binding energy for Ni $2p_{3/2}$ was 854.2 eV, which is characteristic of Ni(II).[34] In the charged state, a satellite structure giving signals at ~863 and ~880 eV was observed in the Ni 2p spectrum (Fig. 5b). These features were previously reported for pristine **P1**[18] and might arise from a charge transfer between nickel and the ligand.[34]

Considering the experimental capacity (220 mA h g^{-1}) and the theoretical capacity of **P1** for a one-electron process (139 mA h g^{-1}),

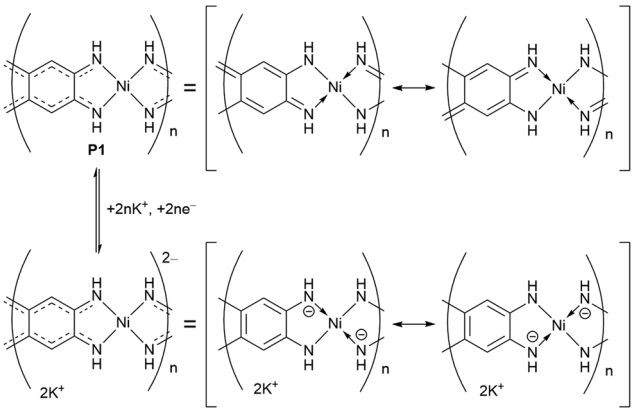

Scheme 1 Proposed overall charge–discharge reaction for **P1**.

as well as the XPS data (Fig. 5), it might be concluded that units of **P1** undergo a two-electron reversible reduction, as displayed in Scheme 1. This reduction mechanism is analogous to that previously reported for lithium batteries in a similar voltage range.[17] Multiple reduction–oxidation peaks observed in the CV (Fig. 3) should be related to phase transitions occurring upon potassiation–depotassiation.

To summarize, we showed that Ni-based coordination polymer derived from 1,2,4,5-tetraaminobenzne can be used as a fast and stable anode for potassium-ion batteries. This study emphasizes the great versatility of organic- and organometallic-based redox-active compounds and features their great potential to be used in different types of batteries due to the facile insertion of Li^+, Na^+, K^+ and probably also other ions. The obtained results encourage further development of amine-derived metal–organic coordination polymers for energy storage applications.

The synthesis and characterization were financially supported by the Russian Science Foundation, project 16-13-00111. P. A. T. acknowledges the support from the Russian Ministry of Science and Education, project 0089-2019-0010. XPS measurements were supported by the Ministry of Education and Science of Russia (Act 211, Agreement No. 02.A03.21.0006 and Theme "Electron" No. AAAA-A18-118020190098-5).

Conflicts of interest

There are no conflicts to declare.

References

1 H. Kim, H. Ji, J. Wang and G. Ceder, *Trends Chem.*, 2019, **1**, 682–692.
2 W. Zhang, Y. Liu and Z. Guo, *Sci. Adv.*, 2019, **5**, eaav7412.
3 J. Zhang, T. Liu, X. Cheng, M. Xia, R. Zheng, N. Peng, H. Yu, M. Shui and J. Shu, *Nano Energy*, 2019, **60**, 340–361.
4 H. Kim, J. C. Kim, M. Bianchini, D.-H. Seo, J. Rodriguez-Garcia and G. Ceder, *Adv. Energy Mater.*, 2018, **8**, 1702384.
5 L. Fan, R. Ma, Q. Zhang, X. Jia and B. Lu, *Angew. Chem., Int. Ed.*, 2019, **58**, 10500–10505.
6 P. Li, J.-Y. Hwang and Y.-K. Sun, *J. Mater. Chem. A*, 2019, **7**, 20675–20682.
7 C. Wang, W. Tang, Z. Yao, B. Cao and C. Fan, *Chem. Commun.*, 2019, **55**, 1801–1804.
8 K. Lei, F. Li, C. Mu, J. Wang, Q. Zhao, C. Chen and J. Chen, *Energy Environ. Sci.*, 2017, **10**, 552–557.

9 J. Han, M. Xu, Y. Niu, G.-N. Li, M. Wang, Y. Zhang, M. Jia and C. m. Li, *Chem. Commun.*, 2016, **52**, 11274–11276.
10 Y. Dong, Z.-S. Wu, S. Zheng, X. Wang, J. Qin, S. Wang, X. Shi and X. Bao, *ACS Nano*, 2017, **11**, 4792–4800.
11 V. Gabaudan, L. Monconduit, L. Stievano and R. Berthelot, *Front. Energy Res.*, 2019, **7**, 46.
12 Z. Chen, I. Belharouak, Y.-K. Sun and K. Amine, *Adv. Funct. Mater.*, 2013, **23**, 959–969.
13 Z. Li, J. Huang, B. Yann Liaw, V. Metzler and J. Zhang, *J. Power Sources*, 2014, **254**, 168–182.
14 S. S. Zhang, K. Xu and T. R. Jow, *J. Power Sources*, 2006, **160**, 1349–1354.
15 S. Wang, W. Quan, Z. Zhu, Y. Yang, Q. Liu, Y. Ren, X. Zhang, R. Xu, Y. Hong, Z. Zhang, K. Amine, Z. Tang, J. Lu and J. Li, *Nat. Commun.*, 2017, **8**, 627.
16 D. Dambournet, I. Belharouak and K. Amine, *Inorg. Chem.*, 2010, **49**, 2822–2826.
17 R. R. Kapaev, S. Olthof, I. S. Zhidkov, E. Z. Kurmaev, K. J. Stevenson, K. Meerholz and P. A. Troshin, *Chem. Mater.*, 2019, **31**, 5197–5205.
18 Y. Chen, M. Tang, Y. Wu, X. Su, X. Li, S. Xu, S. Zhuo, J. Ma, D. Yuan, C. Wang and W. Hu, *Angew. Chem., Int. Ed.*, 2019, **58**, 14731–14739.
19 X. Bie, K. Kubota, T. Hosaka, K. Chihara and S. Komaba, *J. Mater. Chem. A*, 2017, **5**, 4325–4330.
20 K. Chihara, A. Katogi, K. Kubota and S. Komaba, *Chem. Commun.*, 2017, **53**, 5208–5211.
21 F. A. Obrezkov, V. Ramezankhani, I. Zhidkov, V. F. Traven, E. Z. Kurmaev, K. J. Stevenson and P. A. Troshin, *J. Phys. Chem. Lett.*, 2019, **10**, 5440–5445.
22 X. Ren, Q. Zhao, W. D. McCulloch and Y. Wu, *Nano Res.*, 2017, **10**, 1313–1321.
23 Y. Liang, C. Luo, F. Wang, S. Hou, S.-C. Liou, T. Qing, Q. Li, J. Zheng, C. Cui and C. Wang, *Adv. Energy Mater.*, 2019, **9**, 1802986.
24 K. Lei, C. Wang, L. Liu, Y. Luo, C. Mu, F. Li and J. Chen, *Angew. Chem., Int. Ed.*, 2018, **57**, 4687–4691.
25 Q. Zhang, J. Mao, W. K. Pang, T. Zheng, V. Sencadas, Y. Chen, Y. Liu and Z. Guo, *Adv. Energy Mater.*, 2018, **8**, 1703288.
26 Y. Wu, S. Hu, R. Xu, J. Wang, Z. Peng, Q. Zhang and Y. Yu, *Nano Lett.*, 2019, **19**, 1351–1358.
27 I. Sultana, M. M. Rahman, T. Ramireddy, Y. Chen and A. M. Glushenkov, *J. Mater. Chem. A*, 2017, **5**, 23506–23512.
28 P. Xiong, P. Bai, S. Tu, M. Cheng, J. Zhang, J. Sun and Y. Xu, *Small*, 2018, **14**, 1802140.
29 W. Dreyer, J. Jamnik, C. Guhlke, R. Huth, J. Moškon and M. Gaberščček, *Nat. Mater.*, 2010, **9**, 448.
30 P. Gibot, M. Casas-Cabanas, L. Laffont, S. Levasseur, P. Carlach, S. Hamelet, J.-M. Tarascon and C. Masquelier, *Nat. Mater.*, 2008, **7**, 741–747.
31 A. Darwiche, L. Bodenes, L. Madec, L. Monconduit and H. Martinez, *Electrochim. Acta*, 2016, **207**, 284–292.
32 L. Bodenes, A. Darwiche, L. Monconduit and H. Martinez, *J. Power Sources*, 2015, **273**, 14–24.
33 J. Zhao, X. Yang, Y. Yao, Y. Gao, Y. Sui, B. Zou, H. Ehrenberg, G. Chen and F. Du, *Adv. Sci.*, 2018, **5**, 1700768.
34 A. P. Grosvenor, M. C. Biesinger, R. S. C. Smart and N. S. McIntyre, *Surf. Sci.*, 2006, **600**, 1771–1779.

Electronic Supplementary Information

Nickel coordination polymer derived from 1,2,4,5-tetraaminobenzene for fast and stable potassium battery anodes

Roman R. Kapaev,*[abc] Ivan S. Zhidkov,[d] Ernst Z. Kurmaev,[de] Keith J. Stevenson,[a] Pavel A. Troshin[ab]

[a] Center for Energy Science and Technology, Skolkovo Institute of Science and Technology, Nobel str. 3, Moscow 143026, Russia. E-mail: roman.kapaev@skoltech.ru
[b] Institute for Problems of Chemical Physics RAS, Acad. Semenov str. 1, Chernogolovka 142432, Russia
[c] D.I. Mendeleev University of Chemical Technology of Russia, Miusskaya sq. 9, Moscow 125047, Russia
[d] Institute of Physics and Technology, Ural Federal University, Mira str. 19, Yekaterinburg 620002, Russia
[e] M.N. Mikheev Institute of Metal Physics of Ural Branch of Russian Academy of Sciences, S. Kovalevskoi str. 18, Yekaterinburg 620108, Russia

Experimental procedures

Electrode preparation: active material (**P1**), Super P and carboxymethyl cellulose sodium salt with weight ratios of 60:30:10 or 80:10:10 were thoroughly mixed in deionized water to form a homogeneous slurry, which was then tape-cased onto aluminium foil, vacuum-dried at 110 ˚C for 10 h, calendered at room temperature and vacuum-dried again at 110 ˚C for 5 h. Composite mass loading was ~1.7 mg cm^{-2} (**P1** mass loading ~1 mg cm^{-2}) for the electrode with 30% wt. Super P and ~1.6, ~5.0 or 15.2 mg cm^{-2} for the electrodes with 10% wt. Super P. To estimate the contribution to the capacity from Super P, an electrode containing only Super P and carboxymethyl cellulose sodium salt (weight ratio Super P:CMC = 70:30) was prepared according to the same procedure; Super P mass loading for this electrode was ~0.5 mg cm^{-2}.

Cell assembling and testing: Coin cells (CR2032-type) were assembled in a dry argon-filled glovebox with oxygen level below 1 ppm. 1.5м solution of KPF_6 in dry 1,2-dimethoxyethane was used as an electrolyte, potassium metal was used as an anode, glass fiber (Whatman GF/A Glass microfiber filters, GE Healthcare) was used as a separator. Galvanostatic cycling was performed with Neware battery testing systems, cyclic voltammetry was carried out with BioLogic VMP3 potentiostat. Voltage window was 0.5–2.0 V for all cells.

Calculations: Both specific capacities and current densities were calculated basing on the mass of active materials (**P1** for **P1**-based electrodes, Super P for electrodes without **P1**). Coulombic efficiency was calculated as the ratio between charge and discharge capacities.

For **P1**-based electrodes, capacity contribution of Super P (Fig. S1) was subtracted. To do so, charge-discharge curves of Super P at a given current rate were subtracted from the curves of **P1**-based electrodes at the same current rate, considering that the capacity of Super P is proportional to its content in the electrodes.
Particularly, the specific capacity of **P1** (Q_{P1}) was calculated as follows:

$$Q_{P1} = Q^*_{P1} - \frac{w_{SP}}{w_{P1}} Q_{SP}$$

where Q^*_{P1} is the capacity at a given current rate before the subtraction (i.e. absolute battery capacity in mA h divided by the mass of **P1**), Q_{SP} is the capacity of Super P at a given current rate (determined experimentally, calculated per the mass unit of Super P, see Fig. S1), w_{P1} and w_{SP} are weight percentages of **P1** and Super P in the electrodes, respectively (60 and 30 or 80 and 10, depending on the electrode composition).

Since **P1** and Super P have different charge-discharge profiles, it should be noted that the presence of Super P in the electrodes distorts the charge-discharge curves of **P1**. To distinguish the true charge-discharge profiles of **P1**, the following was done:

1. Each charge or discharge curve of **P1** or Super P was represented as an array of XY-pairs, with the potential (ranging from 0.5 to 2.0 V) being the X dimension and the capacity (Q^*_{P1} or $Q_{SP} \times w_{SP} \div w_{P1}$) being the Y dimension.
2. For each pair of arrays (attributed **P1** and Super P), reference subtraction, i.e. subtraction of one curve from another, was performed using OriginPro 2019. The information about the procedure is available at https://www.originlab.com/doc/X-Function/ref/subtract_ref. The Super P arrays were used as the references.
3. X and Y dimensions of the resulting arrays were swapped.

The curves before and after the subtraction are shown in Fig. S2.

In-situ XRD cell preparation and measurements: to prepare the electrode for XRD studies, active material, Super P and poly(vinylidene difluoride) with a weight ratio of 70:20:10 were thoroughly mixed in N-methylpyrrolidone to form a homogeneous slurry, which was then tape-cased onto aluminium foil, vacuum-dried at 110 ˚C for 10 h, calendered at room temperature and vacuum-dried again at 110 ˚C for 5 h. Composite mass loading was ~11 mg cm^{-2} (**P1** mass loading ~7.5 mg cm^{-2}). A Swagelok-type two-electrode cell with a beryllium window was assembled in a dry argon-filled glovebox with oxygen level below 1 ppm. Electrode with the studied material was placed next to the Be window (Al foil in contact with Be), 1.5м solution of KPF_6 in dry 1,2-dimethoxyethane was used as an electrolyte, potassium metal was used as an anode, glass fiber was used as a separator. XRD patterns were measured with Bruker ADVANCE D8 diffractometer, Cu Kα radiation, 2Θ range from 16˚ to 26˚, slit width 1 mm, step 0.06˚, time per step 10 s. The XRD patterns were measured continuously during galvanostatic discharge with the current density of 15 mA g^{-1}, which was performed with BioLogic SP-200.

XPS sample preparation and measurements: coin cells, which were charged/discharged at the current density 50 mA g^{-1}, were disassembled in the Ar-filled glovebox. The electrodes were washed with pure dry 1,2-dimethoxyethane and dried at room temperature. XPS was measured at PHI XPS 5000 VersaProbe spectrometer (ULVAC-Physical Electronics, USA) with a spherical quartz monochromator and an energy analyzer working in the range of binding energies (BE) from 0 to 1500 eV. The energy resolution was $\Delta E \leq 0.5$ eV. The samples were kept in the vacuum chamber for 24 h prior to the experiments and were measured at a pressure bellow 10^{-7} Pa. All spectra were calibrated for external reference Au $4f_{7/2}$ binding energies (84.1 eV). To study the active material itself rather than the SEI layer, Ar^+ ions with 500 eV energy (3 min) were used to eliminate upper SEI layers and reach the subsurface prior to measurements.

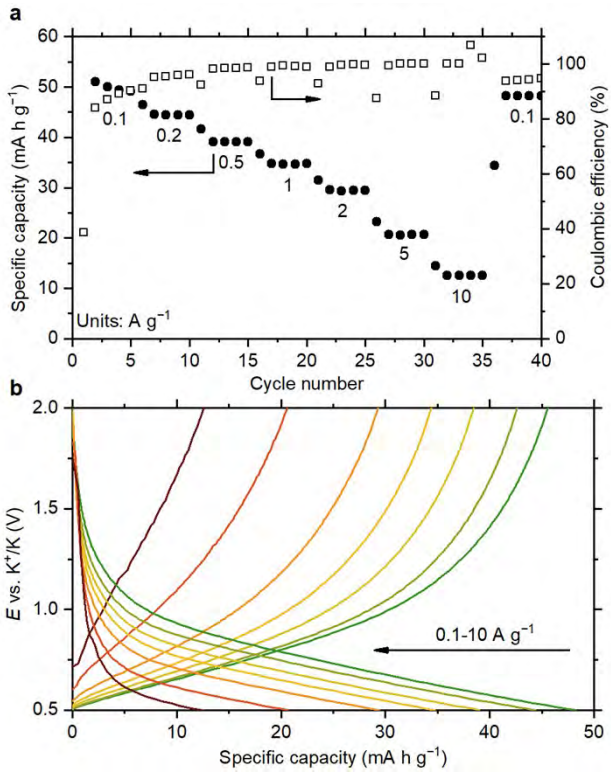

Fig. S1. Rate performance of Super P: (a) specific capacity for different current densities; (b) charge-discharge curves for each 5th cycle shown in (a) except for cycle 5.

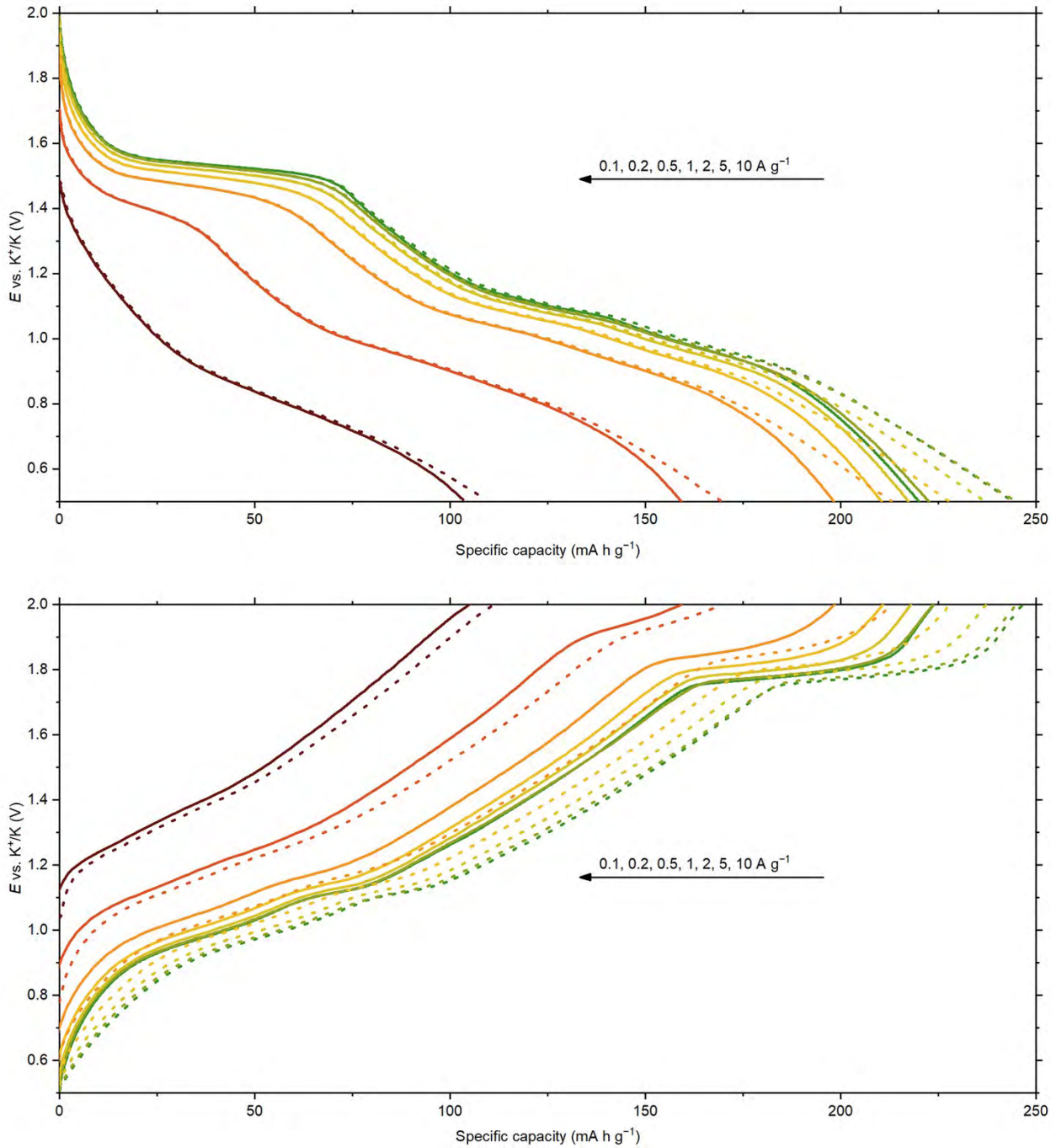

Fig. S2. Discharge (upper plot) and charge (lower plot) profiles at different current rates before (dotted lines) and after (solid lines) subtracting the contribution from Super P.

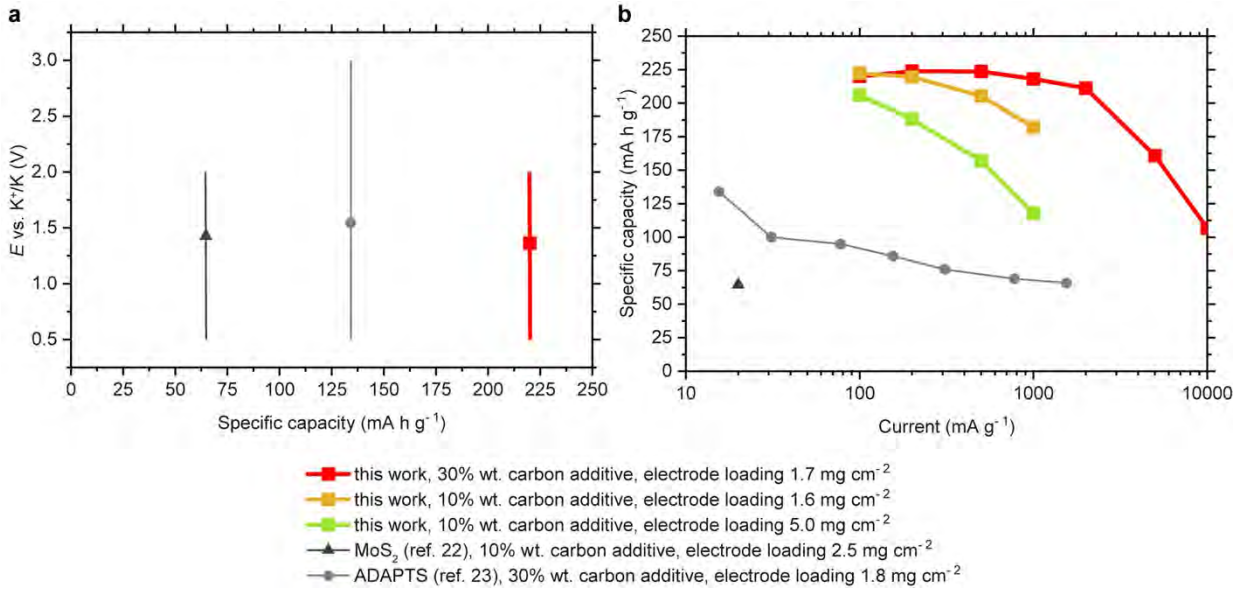

Fig. S3. (a) Working potentials and specific capacities of potassium battery anode materials operating above 0.5 V vs. K^+/K; voltage ranges are shown as lines and average depotassiation potentials are shown as scatter; (b) rate capabilities of the selected materials.

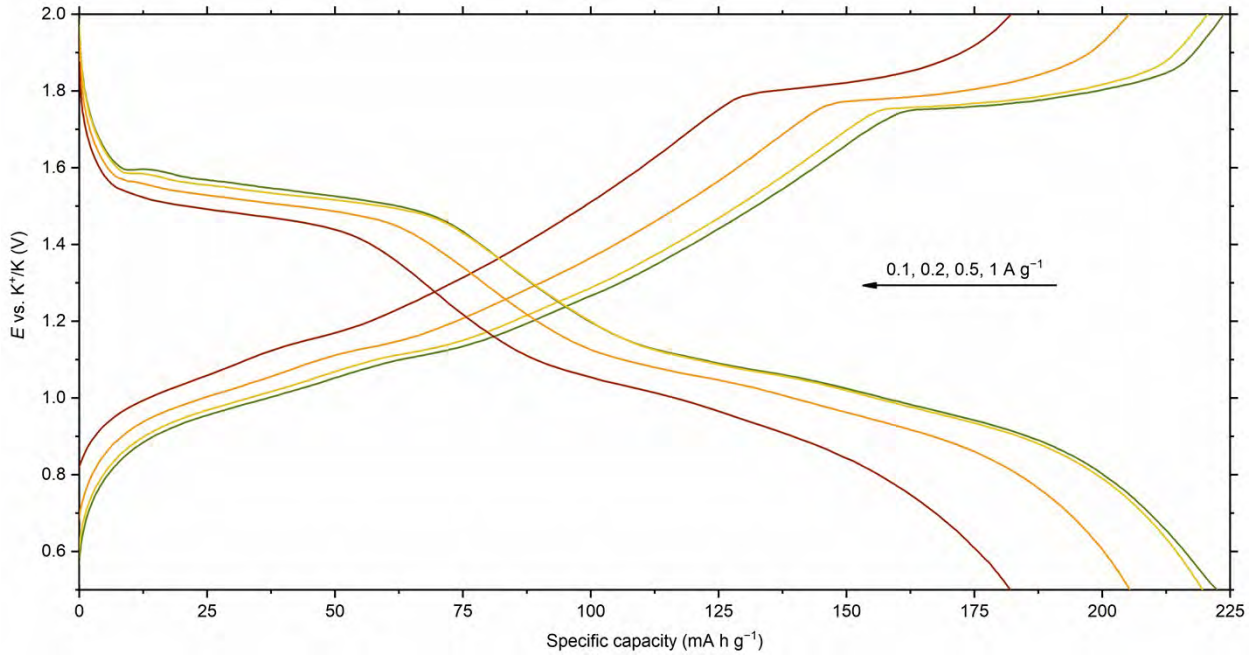

Fig. S4. Charge-discharge profiles of **P1** with 10% wt. Super P at different current densities. Contribution from Super P was subtracted.

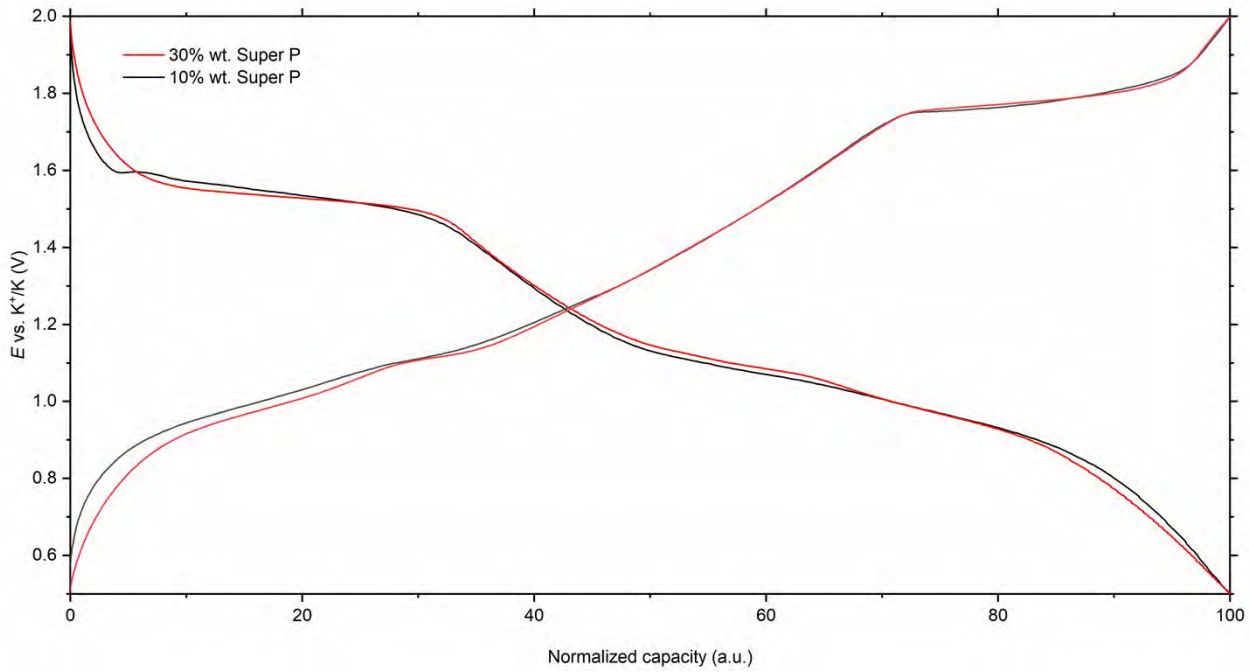

Fig. S5. Charge discharge profiles of **P1** with 10 and 30% wt. Super P at 0.1 A g^{-1}. Contribution from Super P was subtracted.

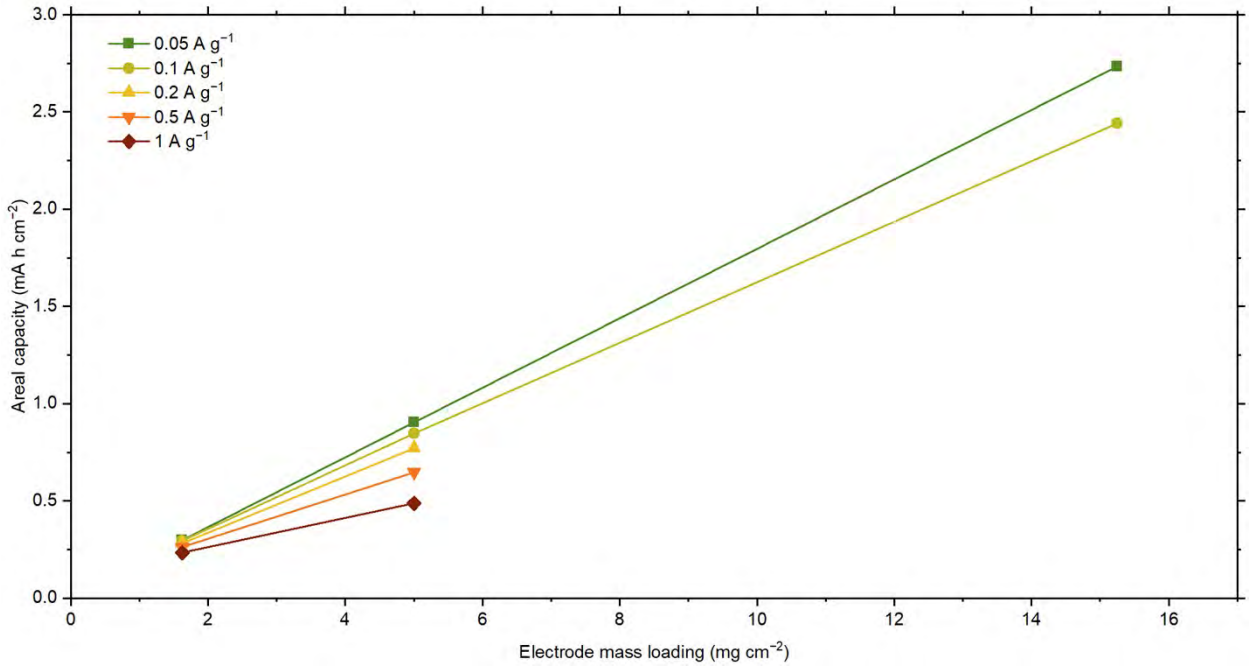

Fig. S6. Areal capacities of **P1**-based electrodes for different electrode loadings and current densities.